nature chemistry

ARTICLES

PUBLISHED ONLINE: 17 MAY 2009 | DOI: 10.1038/NCHEM.212

Room-temperature molecular-resolution characterization of self-assembled organic monolayers on epitaxial graphene

Qing Hua Wang[1] and Mark C. Hersam[1,2]*

Graphene, a two-dimensional sheet of carbon atoms, is a promising material for next-generation technology because of its advantageous electronic properties, such as extremely high carrier mobilities. However, chemical functionalization schemes are needed to integrate graphene with the diverse range of materials required for device applications. In this paper, we report self-assembled monolayers of the molecular semiconductor perylene-3,4,9,10-tetracarboxylic dianhydride (PTCDA) formed on epitaxial graphene grown on the SiC(0001) surface. The molecules possess long-range order with a herringbone arrangement, as shown by ultra-high vacuum scanning tunnelling microscopy at room temperature. The molecular ordering is unperturbed by defects in the epitaxial graphene or atomic steps in the underlying SiC surface. Scanning tunnelling spectra of the PTCDA monolayer show distinct features that are not observed on pristine graphene. The demonstration of robust, uniform organic functionalization of epitaxial graphene presents opportunities for graphene-based molecular electronics and sensors.

Graphene, a two-dimensional hexagonal lattice of carbon atoms, is a material that has attracted significant attention because of its unique electronic structure, high carrier mobilities and quantum relativistic phenomena[1–4]. Although many of these properties have been demonstrated on mechanically exfoliated graphene sheets, epitaxial graphene grown on SiC(0001) surfaces[5–7] is a promising electronic material because it allows for wafer-scale processing and patterning of devices using traditional lithography[8,9]. Epitaxial graphene formed by the thermal decomposition of silicon from SiC(0001) above 1,200 °C has been studied using a wide variety of spectroscopic[10–13] and scanning probe[14–20] techniques. The structure consists of layers of graphene sheets on top of a carbon-rich interfacial layer known as the $(6\sqrt{3} \times 6\sqrt{3})R30^\circ$ reconstruction. The growth mechanism results in a carpet-like coverage of continuous sheets over many SiC steps[15,21]. The presence of the SiC substrate, the interfacial states and various intrinsic defects[22], such as sixfold scattering centres and subsurface carbon nanotubes, may influence the electronic and chemical properties of epitaxial graphene.

To realize its full potential for a diverse range of devices, the bare graphene sheet must be incorporated with other materials. Some initial progress has been made towards the surface functionalization of graphene. In a recent paper by Wang *et al.*[23], atomic-layer deposition of Al_2O_3 was achieved on mechanically exfoliated graphene sheets by functionalizing them with carboxylate-terminated perylene derivatives, and other recent research demonstrated the doping of SiC-grown epitaxial graphene by the deposition of organic molecules[24] and metal atoms[10,11,25,26]. In addition, a recent low-temperature scanning tunnelling microscopy (STM) study found that PTCDA forms a monolayer with a brick-wall structure on epitaxial graphene on SiC(0001) (ref. 27). However, this brick-wall phase of PTCDA was reported as unstable because STM imaging could only be accomplished at 4.7 K, which is an impractical temperature for most applications and subsequent chemistry. Furthermore, the influence of the SiC substrate, the $(6\sqrt{3} \times 6\sqrt{3})R30^\circ$ interface layer and point and line defects on the surface chemistry of epitaxial graphene has not yet been determined.

In this paper, we present a room-temperature molecular-resolution STM investigation of a self-assembled organic monolayer on epitaxial graphene. The organic semiconductor PTCDA was chosen because it has been extensively studied as an archetypical system[28–31] for understanding organic thin films[32–34], and it exhibits ordered layer growth on various substrates, such as silver[35–38], gold[39–41], GaAs(100) (ref. 42) and highly ordered pyrolytic graphite (HOPG)[43–45]. Furthermore, in their recent work, Wang *et al.*[23] used the carboxylic acid derivative of PTCDA to functionalize mechanically exfoliated graphene to introduce reactive sites for the atomic-layer deposition of Al_2O_3. Here, we present the room-temperature self-assembly of PTCDA molecules on epitaxial graphene into stable, well-ordered monolayers arranged in a herringbone phase, with extended domains that span hundreds of nanometres. In addition, the PTCDA monolayer is unperturbed by the presence of the $(6\sqrt{3} \times 6\sqrt{3})R30^\circ$ interface layer, or by surface defects such as atomic steps in the SiC substrate, and point and line defects in the epitaxial graphene. Scanning tunnelling spectroscopy (STS) performed on the PTCDA monolayers showed strong features in the electronic density of states that are distinct from the pristine graphene regions. Overall, this study demonstrates conditions in which robust, uniform, self-assembled organic monolayers can be formed on epitaxial graphene. These monolayers could be used as a template for further chemistry or materials deposition on graphene, enabling the potential fabrication of graphene-based molecular electronic and sensing devices.

Results

Epitaxial graphene. A room-temperature STM image of epitaxial graphene (prepared by graphitization of the SiC(0001) surface) is shown in Fig. 1a. A large terrace of monolayer graphene appears in the centre of the image along with a few scattered defects. Figure 1b is a high-resolution image of monolayer graphene in

[1]Department of Materials Science and Engineering, Northwestern University, Evanston, Illinois 60208, USA, [2]Department of Chemistry, Northwestern University, Evanston, Illinois 60208, USA. *e-mail: m-hersam@northwestern.edu

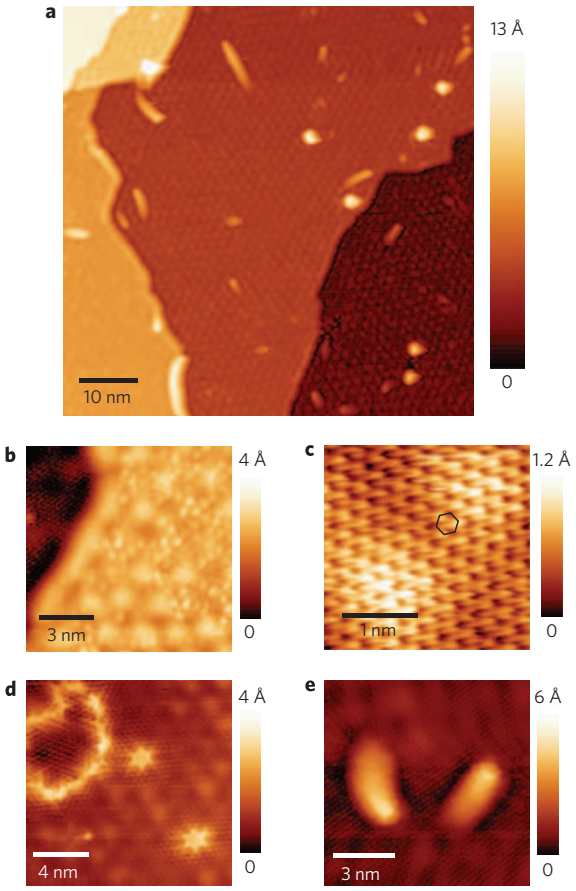

Figure 1 | Epitaxial graphene and its defects. a, STM image of epitaxial graphene grown on SiC(0001) (tunnelling parameters: sample voltage (V_s) = 2.0 V, current (I) = 0.1 nA). The large terrace in the centre of the image is monolayer graphene, and various defects are visible. **b**, High-resolution STM image of monolayer graphene with the underlying $(6\sqrt{3} \times 6\sqrt{3})R30^\circ$ states visible as bright, irregular protrusions ($V_s = -0.5$ V, $I = 0.05$ nA). **c**, Atomic-resolution STM image of bilayer graphene ($V_s = 0.25$ V, $I = 0.02$ nA). The atomic lattice is indicated by the hexagon. **d**, STM image of a loop defect and two sixfold scattering-centre defects ($V_s = 0.25$ V, $I = 0.02$ nA). **e**, Subsurface nanotube defects ($V_s = -0.3$ V, $I = 0.05$ nA).

which the underlying $(6\sqrt{3} \times 6\sqrt{3})R30^\circ$ phase is partially visible through the carbon lattice. A small area of bilayer graphene is shown with atomic resolution in Fig. 1c. The honeycomb atomic structure is indicated by the hexagon overlaid on the image. The inequivalent appearance of adjacent atoms results from the ABAB Bernal stacking between the two graphene sheets[15]. As in a previous report[22], three types of graphene defects were observed: sixfold scattering centres (Fig. 1d), loops formed by the nucleation of scattering centres (Fig. 1d) and subsurface nanotubes (Fig. 1e). We observed that annealing the epitaxial graphene at 1,000 °C for several hours reduced the concentration of loop defects, although the concentration of other types of defects remained unchanged.

Molecular ordering. The PTCDA molecular structure is shown in Fig. 2a. PTCDA is a planar molecule based on a perylene backbone with a conjugated π-electron system and carboxylic acid anhydride side groups. After gas-phase deposition in ultra-high vacuum (UHV), the resultant monolayer of PTCDA on graphene is observed with room-temperature STM (Fig. 2b). The molecule forms a well-ordered, self-assembled monolayer with large domains that span hundreds of nanometres. In Fig. 2b, the same domain extends over the entire image and includes several different steps of various heights. At higher resolution, the herringbone pattern formed by the molecules of the PTCDA monolayer is visible (Fig. 2c). A herringbone pattern has been observed for PTCDA deposited on other substrates, such as Ag(111) (ref. 35), Au(111) (ref. 39) and HOPG[43–45]. This structure closely resembles the (102) plane of the PTCDA bulk crystal structure[28]. Molecular structure diagrams are drawn over the STM image in Fig. 2c to indicate the locations of molecules in the monolayer, and the outline of one unit cell is shown with the lattice vectors **a** and **b** specified. A larger schematic of the monolayer unit cell is shown in Fig. 2d. Molecules at the corner sites of the unit cell appear topographically higher in these tunnelling conditions, which gives the appearance of parallel stripes of brighter and darker molecules that run along the **a** direction, as observed in the large-area STM image of Fig. 2b.

Interactions of the PTCDA monolayer with various types of epitaxial graphene defects are shown in Fig. 2c, e–g. The behaviour of PTCDA at a step edge is shown in Fig. 2c. Here a continuous sheet of graphene has grown over an atomic step in the underlying SiC substrate and the PTCDA monolayer has followed the graphene and continuously flowed over the step. However, when graphene covers two SiC steps in two separate sheets, the PTCDA monolayer is unable to form continuously over both (Fig. 2e). The PTCDA monolayer also continuously flows over the subsurface nanotube defects covered by a continuous sheet of graphene (Fig. 2f). The sixfold scattering-centre defects are difficult to detect under the PTCDA monolayer, but could potentially explain the bright protrusions observed below continuous PTCDA regions (Fig. 2g). These point defects do not perturb the ordering of the PTCDA monolayer.

Submonolayer coverage of PTCDA results in the formation of stable, isolated molecular islands that exhibit the same herringbone arrangement as the full monolayer. In Fig. 3a, a large island of PTCDA is seen in the bottom right portion of the STM image, but the rest of the image is clean graphene. The PTCDA island is shaded blue in Fig. 3b for clarity. Although the islands themselves are stable, their edges show instability that may be caused by the thermal motion of the molecules combined with interactions with the STM tip as it scans over the island boundaries. The atomic-resolution STM image (Fig. 3c) provides a clear view of the boundary of an island. The underlying graphene substrate is on the left side, and the unstable region of the molecular island boundary is on the right side. Despite this instability, the orientation of the molecules is still observable, and when compared with the atomically resolved adjacent graphene, it is apparent that the molecules are not aligned along one of the high-symmetry directions of the substrate. The lack of alignment with the graphene substrate is also shown by the long domain boundary in Fig. 3d, indicated by the large blue arrows. The **a** vectors of the two domains are shown by the thin white arrows, which form an angle of approximately 102° with respect to each other.

The stability and robustness of the PTCDA monolayer is further demonstrated by molecular-resolution STM imaging of this monolayer after removal from UHV (see Supplementary Information). Following exposure to ambient conditions in the laboratory, the monolayer maintains its ordering, and minimal surface contamination is observed.

Scanning tunnelling spectroscopy. The electronic properties of the PTCDA monolayer were characterized using STS. An area of the sample that contained both PTCDA and pristine graphene was chosen (Fig. 4a). The differential tunnelling conductance (dI/dV), which is correlated with the electronic density of states of the sample, was measured as a function of sample-bias voltage for the clean graphene and PTCDA regions, as shown in Fig. 4b,c, respectively. These dI/dV curves were obtained by averaging many individual spectra acquired at random locations within the two square areas

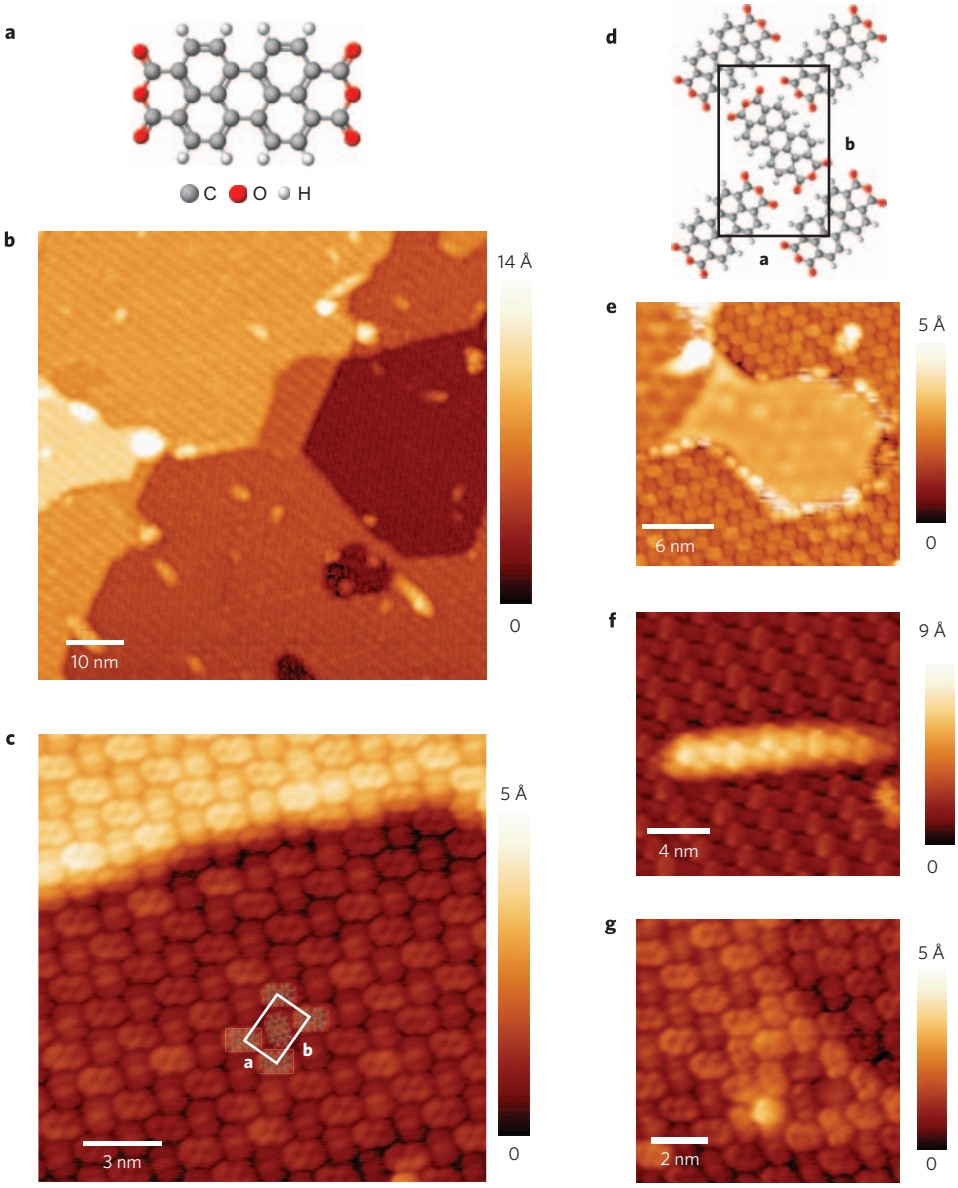

Figure 2 | Self-assembled PTCDA monolayer on the epitaxial graphene substrate. a, Molecular structure of PTCDA. **b**, Monolayer coverage of PTCDA on epitaxial graphene. **c**, Molecular-resolution STM image of the PTCDA monolayer. The PTCDA molecular structure and unit cell outline are overlaid. The monolayer continuously follows the graphene sheet over the SiC step edge. **d**, PTCDA herringbone unit cell, with the lattice vectors **a** and **b** shown. **e**, PTCDA surrounding a step edge where the graphene sheet is not continuous. **f**, PTCDA continuously covers a graphene-subsurface nanotube defect. **g**, A bright protrusion that does not disrupt the PTCDA monolayer and is potentially attributed to a sixfold scattering-centre defect. ($V_s = -2.0$ V, $I = 0.05$ nA for all five STM images.).

outlined in Fig. 4a, which both occur on regions of bilayer graphene. Additional spectra are shown in the Supplementary Information, along with spatial maps of the differential tunnelling conductance. The dI/dV curve for clean graphene (Fig. 4b) features high differential tunnelling conductance at high positive and negative sample biases, and low differential tunnelling conductance at low biases. In contrast, the dI/dV curve for PTCDA (Fig. 4c) possesses a large peak at approximately 1.1 V and a smaller peak at −1.8 V. The differential tunnelling conductance is about zero between about 0.5 V and −1.0 V, and increases at higher biases.

Discussion

The STM and spectroscopy results presented provide insight to the nature of the chemical interaction between the PTCDA molecules and the graphene sheets. The herringbone arrangement of the PTCDA monolayer is similar to that seen on other inert substrates, including graphite, and is also similar to the bulk structure of PTCDA. Consequently, it can be concluded that the interaction between PTCDA and graphene is relatively weak compared with the interaction between molecules. Additional evidence for the primary role of molecule–molecule interactions is the observation of instabilities at molecular domain boundaries, where adjacent molecules are not present to stabilize the monolayer. The herringbone structure is stabilized by hydrogen bonding and quadrupolar interactions between adjacent molecules[45], and π–π^* interactions bind the molecules to the graphene surface.

Despite the similar herringbone arrangement, many differences exist between PTCDA on epitaxial graphene and that on bulk graphite. Although adjacent domains for PTCDA on HOPG have been observed to be rotated by multiples of 60° in previous studies[43,44,46],

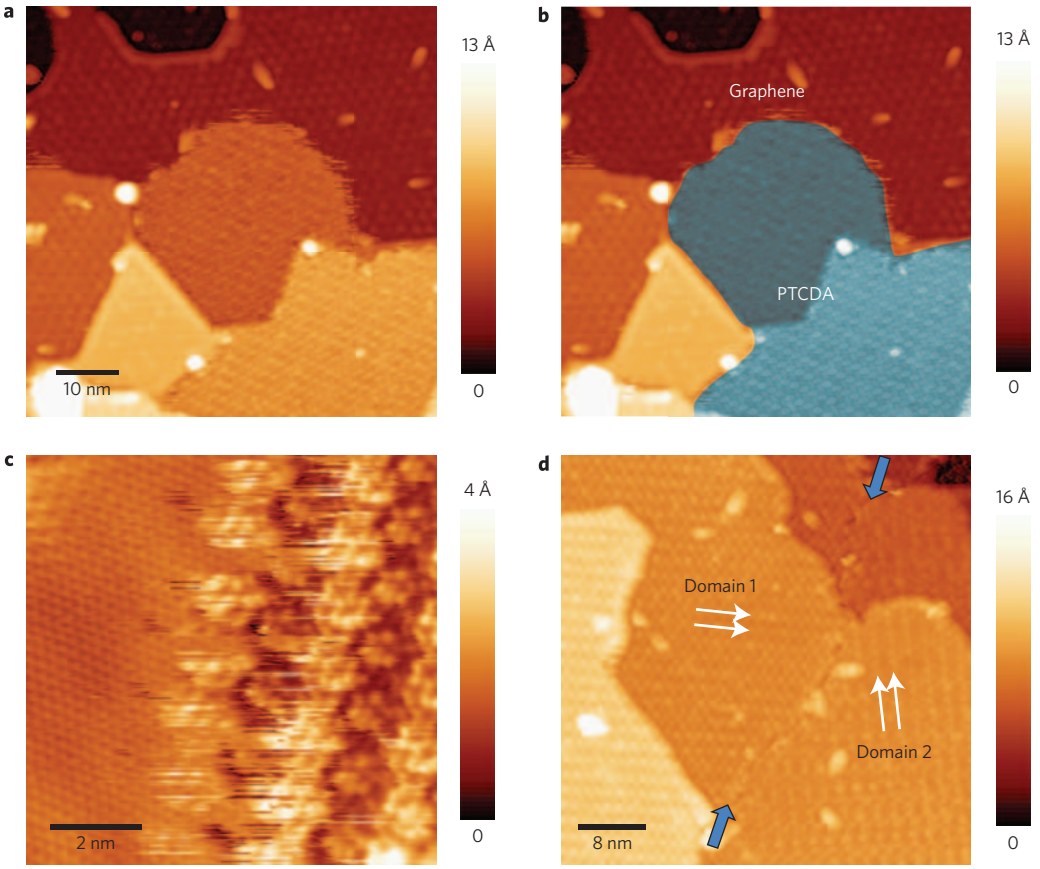

Figure 3 | PTCDA coverage: submonolayer islands and full monolayer domains. a, STM image of a submonolayer coverage of PTCDA on graphene ($V_s = -2.0$ V, $I = 0.05$ nA). The PTCDA island is in the bottom right of the image and the clean graphene substrate is in the remainder of the image. **b**, Same image as (**a**), but with the PTCDA island highlighted in blue for clarity. **c**, High-resolution STM image of a PTCDA island boundary with the atomically resolved graphene substrate on the left half of the image and the PTCDA molecules on the right half ($V_s = 0.25$ V, $I = 0.05$ nA). **d**, STM image showing a domain boundary between two PTCDA domains with different orientations ($V_s = -2.0$ V, $I = 0.05$ nA). Within each domain, the direction of the **a** lattice vector is indicated by thin white arrows. The ends of the domain boundary are indicated by large blue arrows.

systematic rotations between domain boundaries are not detected on epitaxial graphene, which leads to seemingly arbitrary rotations, such as the 102° boundary shown in Fig. 2d. Also, several structural defects not present in graphite are seen in epitaxial graphene, such as the subsurface nanotubes and SiC steps that are covered smoothly by the topmost layer of graphene. The PTCDA monolayer is unaffected by these defects, and is able to form continuously anywhere that the graphene sheet is uninterrupted. Indeed, the PTCDA monolayer has fewer defects than the underlying epitaxial graphene. A similar mode of interaction is theoretically predicted for aromatic molecules on graphene, where π–π^* attractive forces between the molecule and the graphene and hydrogen bonding between the molecules determine the ordering of the adsorbates[47]. Ultimately, the insensitivity of the surface chemistry to the defects in epitaxial graphene implies that uniform self-assembled monolayers can be readily formed on epitaxial graphene surfaces, and thus present a chemically uniform surface for subsequent chemistry or materials deposition.

The STS results show distinct differences between the electronic structure of the PTCDA monolayer and pristine epitaxial graphene. For the PTCDA dI/dV curve, the peaks centred at 1.1 V and −1.8 V can probably be attributed to the lowest unoccupied molecular orbital (LUMO) and highest occupied molecular orbital (HOMO) levels of the PTCDA molecule, respectively. Our results are comparable to previous STS studies of PTCDA monolayers on gold substrates[40,41,48], in which the LUMO level is reported between 0.9 V and 1.3 V, and the HOMO level is reported as approximately −1.9 V. Similarly, for PTCDA on HOPG, these two peaks in the dI/dV curve are measured at 0.7 V and −1.5 V, respectively[45]. The subtle differences in peak positions can be attributed to variations in the setpoint tunnelling conditions of the different experiments, as well as to the work functions of the different substrates. The electronic properties of the PTCDA monolayer are distinct from those of the underlying graphene substrate, and seem to be largely unperturbed by the electronic properties of the epitaxial graphene. These results reinforce the earlier conclusion that PTCDA weakly interacts with the underlying graphene substrate, and is thus insensitive to surface defects.

The STS results do not show strong evidence of surface-transfer doping in the graphene in the presence of the PTCDA monolayer. As the previous low-temperature STM study showed that PTCDA yields a subtle n-type doping effect that is of the order of thermal energy at room temperature[27], it is reasonable to expect that surface transfer doping will not be prominent at room temperature.

Overall, despite the differences that distinguish epitaxial graphene from exfoliated graphene and graphite, particularly the presence of surface defects and the underlying SiC substrate, the self-assembly of PTCDA monolayers closely resembles the behaviour demonstrated on bulk graphite. Furthermore, characterization of the electronic structure of the PTCDA monolayer suggests that the molecule is not substantially perturbed by the electronic structure of epitaxial graphene or the underlying SiC substrate. Consequently, these results suggest that well-ordered, self-assembled monolayers should be readily achievable on epitaxial graphene for the diverse range of

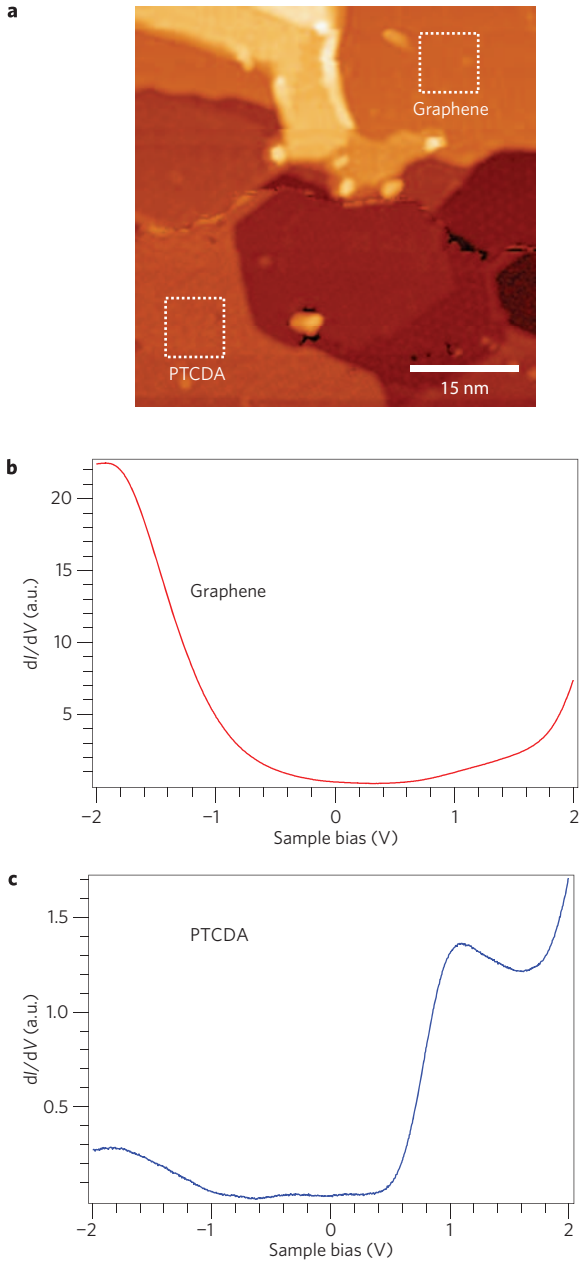

Figure 4 | STS of PTCDA monolayers and clean epitaxial graphene. **a**, STM image showing the sample area in which the spectroscopy was conducted. The upper half of the image is pristine graphene and the lower half is a PTCDA island. The squares indicate areas in which dI/dV spectra were taken at random positions. **b**, dI/dV versus sample bias spectra for clean graphene (a.u., arbitrary units). **c**, dI/dV versus sample bias spectra for the PTCDA monolayer (setpoint: $V_s = 1.0$ V, $I = 0.1$ nA).

adsorbates that have been shown to form monolayers on graphite and related inert surfaces. The extensive body of work exploring the self-assembly of molecules on graphite surfaces should serve as a guide to future studies of self-assembly chemistry on epitaxial graphene. Furthermore, the stability of the PTCDA monolayer upon exposure to ambient conditions suggests opportunities for additional chemistries that can be performed outside the UHV chamber.

Conclusion

In summary, using room-temperature molecular-resolution STM we studied a self-assembled organic monolayer of PTCDA on epitaxial graphene. PTCDA is shown to self-assemble into stable, well-ordered islands and monolayers with a herringbone arrangement at room temperature, which closely resembles its formation on graphite. The PTCDA structures follow the graphene continuously over substrate step edges and other point and line surface defects. At full monolayer coverage, the defect-free molecular domains span hundreds of nanometres, but a submonolayer coverage yields stable, isolated molecular islands. STS results indicate that the electronic structure of the PTCDA monolayer is distinct and largely decoupled from that of the epitaxial graphene or underlying SiC substrate. These results demonstrate that organic functionalization of epitaxial graphene possesses wide tolerance and can be readily achieved at room temperature using surface chemistry analogous to that on bulk graphite. This well-ordered, stable, robust, nearly defect-free monolayer presents opportunities to explore self-assembly chemistry on graphene, to tailor the chemical functionality of graphene and to template growth and deposition of other materials as a potential route towards realizing graphene-based molecular electronic and sensing devices.

Methods

Sample preparation. The sample preparation and STM imaging were conducted in a custom-built UHV STM system with separate sample-preparation and imaging chambers that operated at room temperature and a base pressure of 5×10^{-11} torr (ref. 49). The 6H-SiC(0001) n-type substrates (Cree) were degreased in acetone and isopropanol before being introduced into the vacuum chamber, where they were outgassed overnight at 600 °C. The surface was graphitized by annealing the substrate at 1,250 °C for several cycles of 30 seconds. The substrate was then annealed at 1,000 °C for 2–3 hours and cooled to room temperature before molecular deposition or STM imaging. The cleanliness of the graphene surface was verified by STM imaging, which showed a mixture of monolayer and bilayer graphene, as well as occasional patches of the $(6\sqrt{3} \times 6\sqrt{3})$R30° phase. The substrate was kept at room temperature during molecular deposition and subsequent STM imaging. The PTCDA (97% purity, Sigma-Aldrich) was placed into an alumina-coated tungsten boat and outgassed overnight in the UHV chamber. To deposit the PTCDA onto graphene, the boat was resistively heated to generate a steady molecular flux into which the clean graphene surface was introduced. The PTCDA coverage was controlled by timing the exposure and calibrating the coverage by STM imaging. To remove the PTCDA monolayers, the sample was annealed at 600 °C to recover clean graphene.

Scanning tunnelling microscopy and scanning tunnelling spectroscopy. Topographic STM imaging was conducted in constant-current mode with the bias voltage applied to the sample. Both electrochemically etched tungsten tips and commercially available PtIr tips (Agilent Technologies) were used. STS was conducted by the lock-in detection method, in which a small periodic modulation (0.04 V_{RMS}, 7.5 kHz) was applied to the sample bias and the tunnelling-current response was measured with a lock-in amplifier (Stanford Research Systems) to obtain the differential tunnelling conductance (dI/dV). Spectroscopic data in the form of dI/dV versus sample bias curves were measured by freezing both the tip motion and tunnelling feedback, followed by sweeping the applied sample bias. Many measurements taken at randomly selected spatial locations were averaged (see Supplementary Information) to obtain the curves shown in Fig. 4.

Received 9 January 2009; accepted 6 April 2009; published online 17 May 2009

References

1. Geim, A. K. & Novoselov, K. S. The rise of graphene. *Nature Mater.* **6,** 183–191 (2007).
2. Katsnelson, M. I., Novoselov, K. S. & Geim, A. K. Chiral tunnelling and the Klein paradox in graphene. *Nature Phys.* **2,** 620–625 (2006).
3. Novoselov, K. S. *et al.* Two-dimensional gas of massless Dirac fermions in graphene. *Nature* **438,** 197–200 (2005).
4. Novoselov, K. S. *et al.* Unconventional quantum Hall effect and Berry's phase of 2π in bilayer graphene. *Nature Phys.* **2,** 177–180 (2006).
5. Berger, C. *et al.* Ultrathin epitaxial graphite: 2D electron gas properties and a route toward graphene-based nanoelectronics. *J. Phys. Chem. B* **108,** 19912–19916 (2004).
6. Berger, C. *et al.* Electronic confinement and coherence in patterned epitaxial graphene. *Science* **312,** 1191–1196 (2006).
7. de Heer, W. A. *et al.* Epitaxial graphene. *Solid State Commun.* **143,** 92–100 (2007).
8. Gu, G. *et al.* Field effect in epitaxial graphene on a silicon carbide substrate. *Appl. Phys. Lett.* **90,** 253507 (2007).

9. Kedzierski, J. *et al.* Epitaxial graphene transistors on SiC substrates. *IEEE Trans. Electron Devices* **55,** 2078–2085 (2008).
10. Bostwick, A., Ohta, T., Seyller, T., Horn, K. & Rotenberg, E. Quasiparticle dynamics in graphene. *Nature Phys.* **3,** 36–40 (2007).
11. Ohta, T., Bostwick, A., Seyller, T., Horn, K. & Rotenberg, E. Controlling the electronic structure of bilayer graphene. *Science* **313,** 951–954 (2006).
12. Zhou, S. Y. *et al.* Substrate-induced bandgap opening in epitaxial graphene. *Nature Mater.* **6,** 770–775 (2007).
13. Ni, Z. H. *et al.* Raman spectroscopy of epitaxial graphene on a SiC substrate. *Phys. Rev. B* **77,** 115416 (2008).
14. Brar, V. W. *et al.* Scanning tunneling spectroscopy of inhomogeneous electronic structure in monolayer and bilayer graphene on SiC. *Appl. Phys. Lett.* **91,** 122102 (2007).
15. Lauffer, P. *et al.* Atomic and electronic structure of few-layer graphene on SiC(0001) studied with scanning tunneling microscopy and spectroscopy. *Phys. Rev. B* **77,** 155426 (2008).
16. Poon, S. W., Chen, W., Tok, E. S. & Wee, A. T. S. Probing epitaxial growth of graphene on silicon carbide by metal decoration. *Appl. Phys. Lett.* **92,** 104102 (2008).
17. Riedl, C., Starke, U., Bernhardt, J., Franke, M. & Heinz, K. Structural properties of the graphene–SiC(0001) interface as a key for the preparation of homogeneous large-terrace graphene surfaces. *Phys. Rev. B* **76,** 245406 (2007).
18. Rutter, G. M. *et al.* Scattering and interference in epitaxial graphene. *Science* **317,** 219–222 (2007).
19. Rutter, G. M. *et al.* Imaging the interface of epitaxial graphene with silicon carbide via scanning tunneling microscopy. *Phys. Rev. B* **76,** 235416 (2007).
20. Mallet, P. *et al.* Electron states of mono- and bilayer graphene on SiC probed by scanning-tunneling microscopy. *Phys. Rev. B* **76,** 041403 (2007).
21. Seyller, T. *et al.* Structural and electronic properties of graphite layers grown on SiC(0001). *Surf. Sci.* **600,** 3906–3911 (2006).
22. Guisinger, N. P. *et al.* Atomic-scale investigation of graphene formation on 6H-SiC(0001). *J. Vac. Sci. Technol. A* **26,** 932–937 (2008).
23. Wang, X. R., Tabakman, S. M. & Dai, H. J. Atomic layer deposition of metal oxides on pristine and functionalized graphene. *J. Am. Chem. Soc.* **130,** 8152–8153 (2008).
24. Chen, W., Chen, S., Qi, D. C., Gao, X. Y. & Wee, A. T. S. Surface transfer *p*-type doping of epitaxial graphene. *J. Am. Chem. Soc.* **129,** 10418–10422 (2007).
25. Chen, J. H. *et al.* Charged-impurity scattering in graphene. *Nature Phys.* **4,** 377–381 (2008).
26. Gierz, I., Riedl, C., Starke, U., Ast, C. R. & Kern, K. Atomic hole doping of graphene. *Nano Lett.* **8,** 4603–4607 (2008).
27. Lauffer, P., Emtsev, K. V., Graupner, R., Seyller, T. & Ley, L. Molecular and electronic structure of PTCDA on bilayer graphene on SiC(0001) studied with scanning tunneling microscopy. *Phys. Status Solidi B* **245,** 2064–2067 (2008).
28. Forrest, S. R. Ultrathin organic films grown by organic molecular beam deposition and related techniques. *Chem. Rev.* **97,** 1793–1896 (1997).
29. Forrest, S. R. Organic–inorganic semiconductor devices and 3, 4, 9, 10 perylenetetracarboxylic dianhydride: an early history of organic electronics. *J. Phys. Condens. Matter* **15,** S2599–S2610 (2003).
30. Tautz, F. S. Structure and bonding of large aromatic molecules on noble metal surfaces: the example of PTCDA. *Prog. Surf. Sci.* **82,** 479–520 (2007).
31. Hirose, Y. *et al.* Chemistry and electronic properties of metal–organic semiconductor interfaces: Al, Ti, In, Sn, Ag, and Au on PTCDA. *Phys. Rev. B* **54,** 13748–13758 (1996).
32. Shirota, Y. Organic materials for electronic and optoelectronic devices. *J. Mater. Chem.* **10,** 1–25 (2000).
33. Forrest, S. R. The path to ubiquitous and low-cost organic electronic appliances on plastic. *Nature* **428,** 911–918 (2004).
34. Dimitrakopoulos, C. D. & Malenfant, P. R. L. Organic thin film transistors for large area electronics. *Adv. Mater.* **14,** 99–117 (2002).
35. Eremtchenko, M., Schaefer, J. A. & Tautz, F. S. Understanding and tuning the epitaxy of large aromatic adsorbates by molecular design. *Nature* **425,** 602–605 (2003).
36. Rohlfing, M., Temirov, R. & Tautz, F. S. Adsorption structure and scanning tunneling data of a prototype organic–inorganic interface: PTCDA on Ag(111). *Phys. Rev. B* **76,** 115421 (2007).
37. Kraft, A. *et al.* Lateral adsorption geometry and site-specific electronic structure of a large organic chemisorbate on a metal surface. *Phys. Rev. B* **74,** 041402 (2006).
38. Glockler, K. *et al.* Highly ordered structures and submolecular scanning tunnelling microscopy contrast of PTCDA and DM-PBDCI monolayers on Ag(111) and Ag(110). *Surf. Sci.* **405,** 1–20 (1998).
39. Schmitz-Hübsch, T., Fritz, T., Sellam, F., Staub, R. & Leo, K. Epitaxial growth of 3,4,9,10-perylene-tetracarboxylic-dianhydride on Au(111): a STM and RHEED study. *Phys. Rev. B* **55,** 7972–7976 (1997).
40. Nicoara, N., Roman, E., Gomez-Rodriguez, J. M., Martin-Gago, J. A. & Mendez, J. Scanning tunneling and photoemission spectroscopies at the PTCDA/Au(111) interface. *Org. Electron.* **7,** 287–294 (2006).
41. Toerker, M., Fritz, T., Proehl, H., Sellam, F. & Leo, K. Tunneling spectroscopy study of 3,4,9,10-perylenetetracarboxylic dianhydride on Au(100). *Surf. Sci.* **491,** 255–264 (2001).
42. Nicoara, N. *et al.* Scanning tunnelling microscopy and spectroscopy on organic PTCDA films deposited on sulfur passivated GaAs(001). *J. Phys. Condens. Matter* **15,** S2619–S2629 (2003).
43. Hoshino, A., Isoda, S., Kurata, H. & Kobayashi, T. Scanning tunneling microscope contrast of perylene-3,4,9,10-tetracarboxylic-dianhydride on graphite and its application to the study of epitaxy. *J. Appl. Phys.* **76,** 4113–4120 (1994).
44. Kendrick, C., Kahn, A. & Forrest, S. R. STM study of the organic semiconductor PTCDA on highly-oriented pyrolytic. *Appl. Surf. Sci.* **104/105,** 586–594 (1995).
45. Ludwig, C., Gompf, B., Petersen, J., Strohmaier, R. & Eisenmenger, W. STM investigations of PTCDA and PTCDI on graphite and MoS_2—A systematic study of epitaxy and STM image-contrast. *Z. Phys. B: Condens. Matter* **93,** 365–373 (1994).
46. Forrest, S. R., Burrows, P. E., Haskal, E. I. & So, F. F. Ultrahigh-vacuum quasiepitaxial growth of model van der Waals thin films. II. Experiment. *Phys. Rev. B* **49,** 11309–11321 (1994).
47. Rochefort, A. & Wuest, J. D. Interaction of substituted aromatic compounds with graphene. *Langmuir* **25,** 210–215 (2009).
48. Tsiper, E. V., Soos, Z. G., Gao, W. & Kahn, A. Electronic polarization at surfaces and thin films of organic molecular crystals: PTCDA. *Chem. Phys. Lett.* **360,** 47–52 (2002).
49. Foley, E. T., Yoder, N. L., Guisinger, N. P. & Hersam, M. C. Cryogenic variable temperature ultrahigh vacuum scanning tunneling microscope for single molecule studies on silicon surfaces. *Rev. Sci. Instrum.* **75,** 5280–5287 (2004).

Acknowledgements

This work was supported by the National Science Foundation and the Office of Naval Research. The authors thank N. Guisinger for discussions and J. Lyding for use of his STM control software.

Author contributions

Q.H.W. and M.C.H. conceived the experiments, analysed the data and co-wrote the manuscript. Q.H.W. performed the experiments.

Additional information

Supplementary information accompanies this paper at www.nature.com/naturechemistry. Reprints and permission information is available online at http://npg.nature.com/reprintsandpermissions/. Correspondence and requests for materials should be addressed to M.C.H.